IEEE Access
Multidisciplinary | Rapid Review | Open Access Journal

Received November 5, 2019, accepted November 19, 2019, date of publication November 26, 2019,
date of current version December 10, 2019.

Digital Object Identifier 10.1109/ACCESS.2019.2956102

Real-Time Rendering Method of Depth-Image-Based Multiple Reference Views for Integral Imaging Display

YANXIN GUAN[1], XINZHU SANG[1], SHUJUN XING[2], YUANHANG LI[1], AND BINBIN YAN[1]
[1]State Key Laboratory of Information Photonics and Optical Communications, Beijing University of Posts and Telecommunications (BUPT), Beijing 100876, China
[2]State Key Laboratory of Precision Measurement Technology and Instruments, Tsinghua University, Beijing 100084, China

Corresponding authors: Xinzhu Sang (xzsang@bupt.edu.cn) and Binbin Yan (yanbinbin@bupt.edu.cn)

This work was supported in part by the National Key Research and Development Program under Grant 2017YFB1002900, in part by the National Natural Science Foundation of China under Grant 61705014 and Grant 61575025, and in part by the Fundamental Research Funds for the Central Universities under Grant 2019RC13 and Grant 2019PTB-018.

ABSTRACT A real-time computer-generated integral imaging (CGII) display rendering method based on depth-image-based multiple reference viewpoints (MDIBR) is presented, and good three-dimensional (3D) image quality with the high frame rate can be achieved. The traditional rasterization pipeline and 3D image warping are used to accelerate CGII, and the proposed method is suitable for dynamic and complex 3D content generation for the 3D display. Qualitative and quantitative experiments are carried out to evaluate the feasibility of the proposed method. Experimental results show that the MDIBR method can achieve real-time integral imaging display with 80 × 80 viewpoints based on large-scale 3D data with a million points.

INDEX TERMS 3D display, integral imaging, real-time rendering, computer generated integral imaging.

I. INTRODUCTION

Recently, 3D displays have attracted considerable attention [1]. The autostereoscopic technique based on integral imaging can display full-color 3D images with effectively continuous horizontal and vertical motion parallax [2]–[5]. Currently, the CGII is prominent and widely used for the integral imaging display system, and the elemental image array (EIA) can be achieved with a virtual lens array whose parameters are determined by the real lens array of the integral imaging display.

Several efficient CGII methods have been presented, such as point retracing rendering (PRR) [6], [7], multiple viewpoint rendering (MVR) [8], [9], parallel group rendering (PGR) [10], [11], viewpoint vector rendering (VVR) [12]–[14], image space parallel processing (ISPC) [15], [16], multiple ray cluster rendering (MRCR) [17], multiple orthographic frustum combing (MOFC) [18], and backward ray-tracing (BRT) [19], [20]. PRR is the simplest elementary image-mapping algorithm, but the heavy calculation required is time-consuming, which makes it unsuitable for real-time processing. For MVR, each elemental image is sequentially generated by rendering the perspective image with the corresponding virtual lens, and the computational time increases linearly with the number of the lens. PGR is a more efficient algorithm and the EIA is obtained from the directional scenes, with the small rendering number of scenes passing to the number of displayed pixels in one elemental image. VVR can be suitable for all display modes but it is time-consuming, and heavier computation is required with an increasing number of viewpoints. A real-time user-interactive integral imaging 3D display system can be realized for 3D volume data based on ISPC. Both MRCR and MOFC require duplication of 3D content, and they are limited to small 3D scenes and EIAs. A high-quality integral image can be created with BRT, but it is not suitable for dynamic scenes.

Image-based modeling and rendering techniques are a powerful alternative method to traditional geometry-based techniques for image synthesis [21], [22]. Instead of geometric primitives, a collection of sample images are used to render novel views. The depth-image-based rendering (DIBR) technique is widely used to synthesize virtual views in many applications including multi-view and free-viewpoint video systems [23]. Traditional DIBR can quickly generate multi-view images, but its inherent problem is that holes appear

The associate editor coordinating the review of this manuscript and approving it for publication was Sudipta Roy.

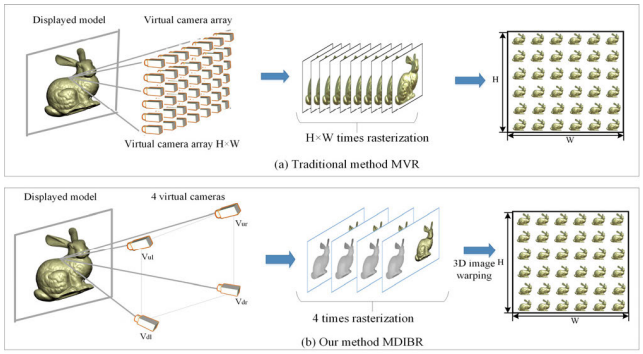

FIGURE 1. The process of (a) the traditional method MVR and (b) our method MDIBR.

in the synthesized view [24], [25]. Therefore, various hole-filling algorithms have been proposed [26], [28]. For real-time rendering of the virtual scene, the depth map is accurate and easy to obtain, which can make better use of image-based rendering.

Here, the efficient CGII method of MDIBR is presented, and an interactive integral imaging display system is realized with multiple 3D data. A GPU is used to generate dense-view images in parallel. Compared with the traditional DIBR method, the generated virtual viewpoint image has fewer holes, and the occlusion relations among the virtual objects are more accurate. In the experiment, up-left, down-left, up-right and down-right viewpoints are used as reference viewpoints. A 3D scene with millions of vertices can be processed and displayed at 25 frames per second with 3840 × 2160 resolution.

II. MDIBR METHOD

In CGII, the multi-viewpoint image generation is an important factor for the calculation speed. In traditional methods such as MVR, the image of different viewpoints is generated with cameras in different positions. The disadvantage of the MVR method is that the computation time is proportional to the number of viewpoints. As shown in Figure 1(a), when the number of viewpoints is H×W, the total number of iterations is H×W, and the time is H×W times greater than that of a single viewpoint. In our method MDIBR as shown in Figure 1(b), the up-left, down-left, up-right and down-right viewpoints are used as reference viewpoints, which are generated based on the rasterization pipeline, and other viewpoints are generated with the 3D image warping process. The 3D image warping is a GPU-based image processing technique, and its calculation is independent of the number of viewpoints. Therefore, MDIBR is efficient for integral imaging with a large number of viewpoints.

The basic steps of the MDIBR procedure are illustrated in Figure 2. Firstly, 3D models in the virtual scene along with positions and orientations of the virtual camera are set. With the traditional rasterization rendering process, the depth and 2D images for the reference are obtained. Then, images of intermediate viewpoints can be interpolated through 3D

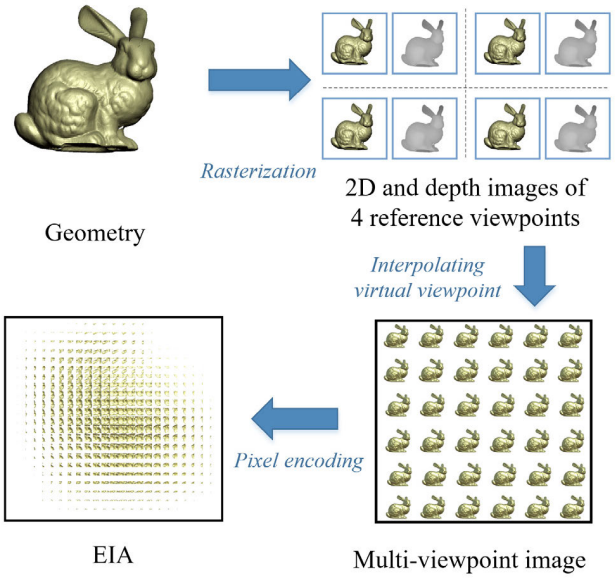

FIGURE 2. The rendering pipeline of MDIBR.

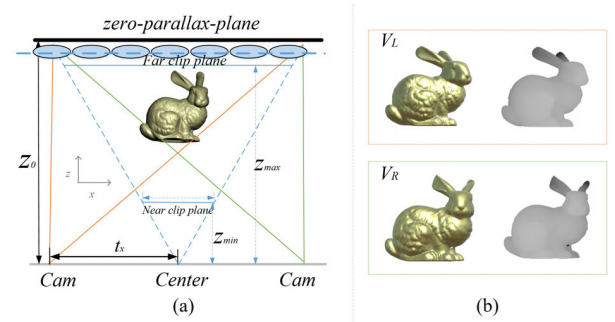

FIGURE 3. Generation of depth and 2D images: (a) the cameras in the virtual world; (b) the 2D and depth image by rasterization.

warping with 2D and depth images. Finally, the textures of intermediate virtual viewpoints are used to synthesize the EIA. Here, the generation of dense-view images is focused.

A. DEPTH AND 2D IMAGES OF THE REFERENCE VIEWPOINT

In the common rasterization rendering technology, the obtained 3D information in the virtual scene can be converted into a 2D image and a depth image with the virtual pinhole camera model. As shown in Figure 3(a), two cameras are set in the horizontal direction according to the viewpoints in the real world. After rasterization rendering, 2D images and depth images of two viewpoint positions are obtained, as shown in Figure 3(b). The projection matrix $\boldsymbol{P}$ of the virtual camera needs to be shear transformed, and its shear matrix $\boldsymbol{M}_{\mathbf{shear}}$ is shown in (1) [29]. t_x and t_y are the distances between the point of view and the center on the zero-parallax-plane in the x and y directions respectively, and z_0 is the z-axial distance between the zero-parallax-plane and the point of view. $\boldsymbol{M}_{\mathbf{projection}}$ with the shear transform is given by the (2), which can cause an off-axis perspective [30]. $\boldsymbol{P}$ is a traditional perspective projection matrix. Here,z_{min} is the nearest clip

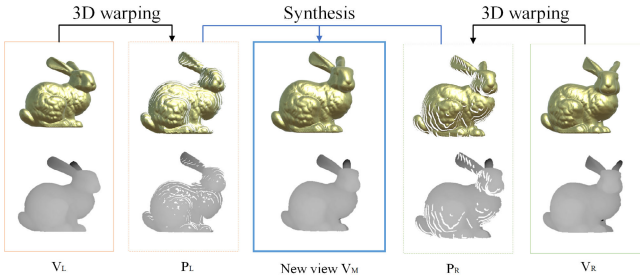

FIGURE 4. Synthesis process of new viewpoint images by 3D image warping.

plane distance and z_{max} is the farthest clip plane distance. *width* and *height* represent the width and height of near the clip plane respectively. Different from the DIBR method, depth images and 2D images of multiple viewpoints are collected as references to synthesize new viewpoints for the proposed method.

$$\boldsymbol{M}_{\mathbf{shear}} = \begin{bmatrix} 1 & 0 & -\dfrac{\mathbf{t}_x}{z_0} & 0 \\ 0 & 1 & -\dfrac{\mathbf{t}_y}{z_0} & 0 \\ 0 & 0 & 1 & 0 \\ 0 & 0 & 0 & 1 \end{bmatrix} \tag{1}$$

$$\begin{aligned} \boldsymbol{M}_{\mathbf{projection}} &= \boldsymbol{M}_{\mathbf{shear}}\boldsymbol{P} \\ &= \boldsymbol{M}_{\mathbf{shear}} \begin{bmatrix} \dfrac{2z_{\min}}{width} & 0 & 0 & 0 \\ 0 & \dfrac{2z_{\min}}{height} & 0 & 0 \\ 0 & 0 & -\dfrac{z_{\max}+z_{\min}}{z_{\max}-z_{\min}} & \dfrac{2z_{\max}z_{\min}}{z_{\max}-z_{\min}} \\ 0 & 0 & -1 & 0 \end{bmatrix} \end{aligned} \tag{2}$$

B. INTERPOLATING VIRTUAL VIEWPOINT

Concatenation of re-projection (2D-to-3D) and the subsequent projection (3D-to-2D) are usually called 3D image warping, which is a common method to generate virtual viewpoints [23]. The 3D warping method is improved in two parts. On the one hand, the number of reference viewpoints is increased to obtain more 3D spatial information. On the other hand, the previous frame is used to fill the hole in the destination viewpoint. The algorithm requires multiple reference viewpoints with multiple times of 3D warping. As shown in Figure 4, the new viewpoint images P_L and P_R including visible holes are warped from the reference images V_L and V_R. Multiple reference images can be composited to produce a more complete image that can meet the expectations. The pixel with the minimum depth from P_L and P_R is selected to fill the pixel in the destination viewpoint. The complete image in the new viewpoint V_M is composited by P_L and P_R.

To guarantee the efficiency and quality of the 3D image, the hole filling method is proposed as shown in Figure 5.

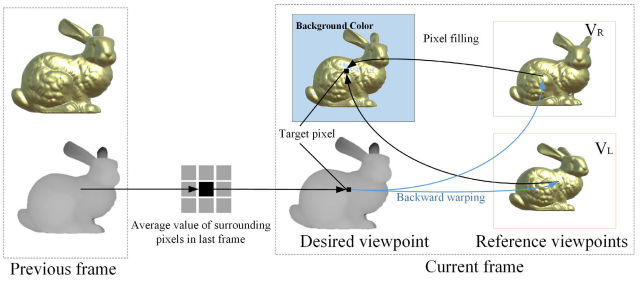

FIGURE 5. The process of hole filling.

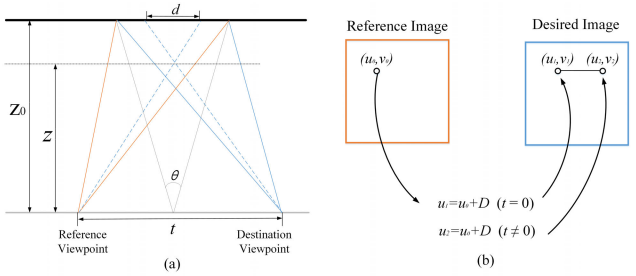

FIGURE 6. 3D image warping. (a) Correspondence between pixels of a reference image and destination image. (b) Disparity in the screen coordinate system.

When hole appears, the depth image of the previous frame can be used to backward warping, and the color value of the target pixel can be found in the reference viewpoint V_L or V_R to fill in the hole position of the hole desired viewpoint. If the target pixel of the same index in the previous frame is also in hole, the average value of the pixels around the target pixel in the previous frame is used to be the depth value of the target viewpoint. In addition, the pixels with maximum depth are filled by the background color.

Conceptually, the new view generation can be interpreted as the following two steps. At first, original image points are re-projected into the 3D world based on the respective depth data. Then, these 3D space points are projected into the image plane of a ''virtual'' camera, which is located at the required viewing position. As shown in Figure 6(a), pixels in the destination image are corresponded one by one, and the basic mapping rule conforms to the following (3),

$$\frac{z_0 - z}{z} = \frac{d}{t}, \tag{3}$$

where z represents the normalized depth value, and d denotes the disparity between the destination image and its image in the world coordinate system. Finally, the pixel disparity in the screen world D can be expressed as follows,

$$D = floor\left(\frac{L \cdot z_0}{d}\tan\frac{\theta}{2}\right), \tag{4}$$

where *the floor* represents a truncation function that maps a real number to the largest previous integer, θ is the horizontal field of view of the virtual camera and L denotes the horizontal resolution of the reference image. The pixel position in the desired image can be calculated by the index in the reference image and the pixel position offset D, as shown in Figure 6(b).

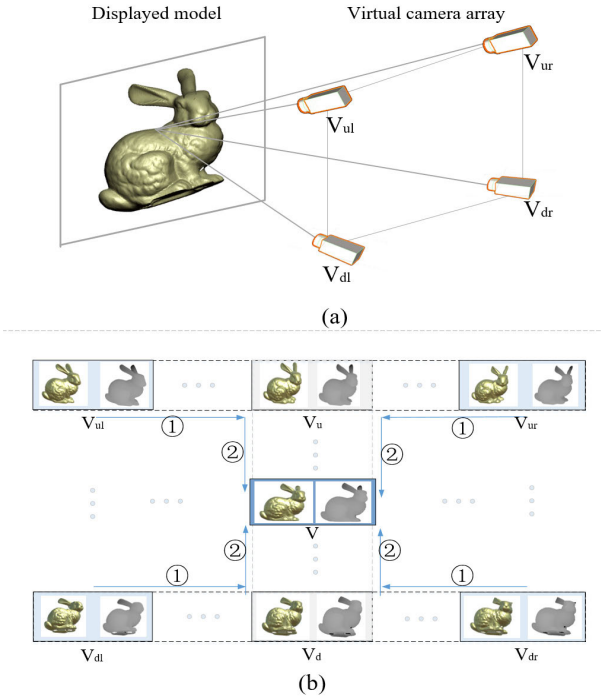

FIGURE 7. (a) Reference images sampled with camera array; (b) 3D warping in full parallax.

The EIA for integral imaging light field display is with parallax in both directions, and 3D warping should be performed in both the horizontal and vertical directions. The 2D and depth images of 4 viewpoints are used as references. Locations of the cameras are shown in Figure 7(a) where four virtual cameras are used.

As shown in Figure 7(b), generation of the new viewpoint images contains two 3D warping processes. Here, up-left viewpoint V_{ul}, down-left viewpoint V_{dl}, up-right viewpoint V_{ur} and down-right viewpoint V_{dr} are used as reference viewpoints. Firstly, the image of up viewpoint V_u is warped from viewpoint V_{ul} and V_{ur}, and the image of down viewpoint V_d is warped from viewpoint V_{dl} and V_{dr}. Secondly, the image of the target viewpoint V is warped from V_u and V_d.

The two 3D warping processes are performed independently. To be suitable for the light field display, the resulting picture needs to be shear transformed, which is different from the traditional 3D warping method. The effect of the conventional 3D warping method is to match the effect of the parallel camera. The 3D warping effect in this paper is to match the effect of the off-axis camera. We can also perform vertical warping first and then horizontal warping. When this step is completed, a multi-viewpoint image can be obtained as shown in Figure 8.

C. PIXEL ENCODING FOR EIA

For the proposed algorithm, after the 3D image warping step, the EIA is generated by interleaving the multi-viewpoint image in a pixel mapping process, as shown in Figure 8. Here, the common pixel mapping scheme is used [18]. The pixel in

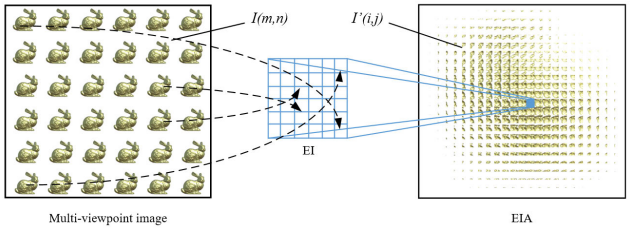

FIGURE 8. Schematic of the pixel mapping process in the MDIBR method.

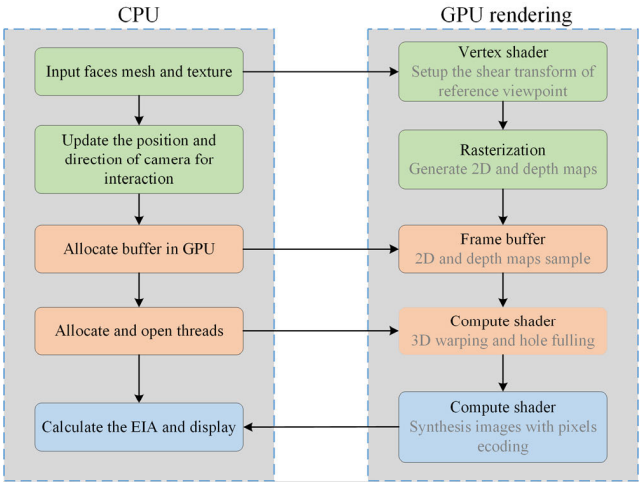

FIGURE 9. Flowchart of the proposed MDIBR method on GPU.

the mth column and the nth row of the multi-viewpoint image is denoted as $I(\mathrm{m}, n)$, and the pixel $I(\mathrm{m}, n)$ is mapped to the ith column and the jth row pixel in the EIA, which is denoted as $I'(i, j)$. Thus, we can obtain the equation as

$$I'(i, j) = I(m, n). \tag{5}$$

The relationship between i, j, m, and n can be obtained:

$$i = \left[mod(m, \frac{L_h}{p}) + 1 \right] \times r - floor(m \times \frac{\mathrm{p}}{L_h}) - 1, \tag{6}$$

$$j = \left[mod(n, \frac{L_v}{p}) + 1 \right] \times r - floor(n \times \frac{\mathrm{p}}{L_v}) - 1, \tag{7}$$

where the function mod denotes the modulo operator. With the above rendering parameters, a multi-view image is generated with the image resolution of $floor(L_h/p_d)$ in the horizontal direction and $floor(L_v/p_d)$ in the vertical direction. p_d is a pitch of the display panel. L_h and L_v respectively stand for the length of the whole lens array in horizontal and vertical directions.

D. RAPID CALCULATION ON GPU

Parallelization is important to achieve real-time generation. The MDIBR algorithm with high parallelism is well suited for accelerating calculations with GPUs. The number of threads used in GPU is related to the number of viewpoints and the resolution of a single viewpoint. For example, if N virtual viewpoints with W×H resolution are to be generated,

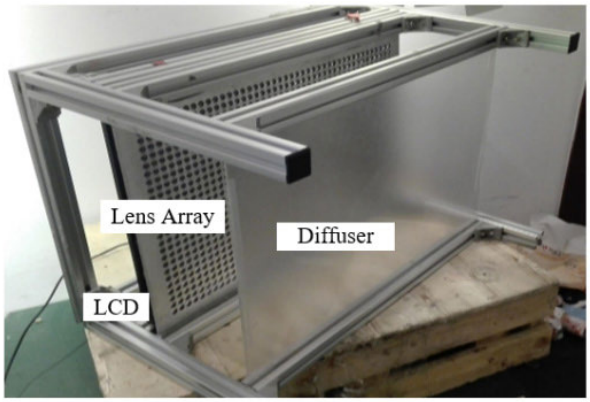

FIGURE 10. The photograph of integral imaging display system.

TABLE 1. Related parameters of integrated imaging display system.

Parameter	Value
Resolution	3840×2160
Number of views	80×80
Field of view	40°
Viewing distance	2m

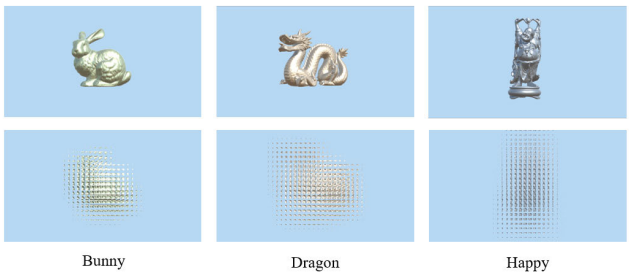

FIGURE 11. The images generated by center camera and EIA.

N×W×H threads are required in GPU. To avoid memory conflict, we use atomic operation and thread synchronization in GPU calculation. The illustration of our GPU-accelerated pipeline is shown in Figure 9. The green blocks represent rasterization, which is already introduced in 2.1. Reference images are parallel computed with the traditional rasterization rendering pipeline. Orange blocks represent the 3D image warping process introduced in 2.2, and the blue ones represent the image synthesis process introduced in 2.3. Finally, the EIA is generated in the display system.

III. EXPERIMENTAL RESULTS

A. EXPERIMENTAL CONFIGURATION

Here, a dense-viewpoint integral imaging display shown in Figure 10 is used, and its numerical parameters in the experiment are summarized in Table 1. In the experiments, a computer with a CPU Intel(R) Core(TM) i7-4790K@3.60GHz and NVIDIA GeForce GTX970 graphic card plays a significant role in the generation process. The algorithm is implemented with the help of OpenGL and GLSL shading languages.

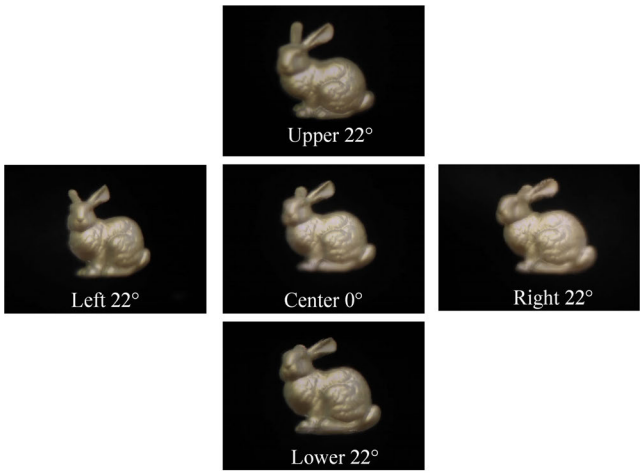

FIGURE 12. Different perspectives of the reconstructed 3D scene on light field display.

TABLE 2. The frame rate.

Model	Vertices	Triangles	Speed(FPS)
Bunny	135067	69451	33
Dragon	1387319	871306	30
Happy	1855994	1087474	25

B. PERFORMANCE EVALUATION

Several different virtual 3D objects are generated for testing the performance of the proposed method as shown in Figure 11. The patch and vertex parameters of the 3D objects are illustrated in Table 2. The real-time generation frame rate of the EIAs is above 25 fps. Figure 12 shows the display effect of the 3D mesh model "Bunny" in different directions on the integral imaging display system.

To show the real-time rendering ability of the algorithm, an animated cat mesh model is used to test the real-time rendering performance, as shown in Visualization1. There are 4022 and 7298 triangle faces for the cat model. The reconstructed image on the integrated imaging field is consistent with the original image, and the average frame rate is 45fps. The average time of rendering a frame is about 22ms, and it takes 18ms for 3D warping with hole fulling.

The proposed MDIBR method is compared with the previous real-time CGII method. The MDIBR method and the MVR method are compared with different numbers of the EIA. The frame rates of the two methods for mesh models of three different sizes are respectively presented in Figures 13(a) and 13(b). MDIBR is more efficient than MVR, especially in the case of a larger number of viewpoints. The performance of MDIBR is tested with vertex numbers and resolutions in dynamic and static scenes, and compared with the BRT method. Figs. 13(c) and 13(d) indicate that MDIBR is more efficient than BRT, especially in dynamic scenes.

C. IMAGE QUALITY EVALUATION

The structural similarity (SSIM) index is a method for predicting the perceived quality of digital television and

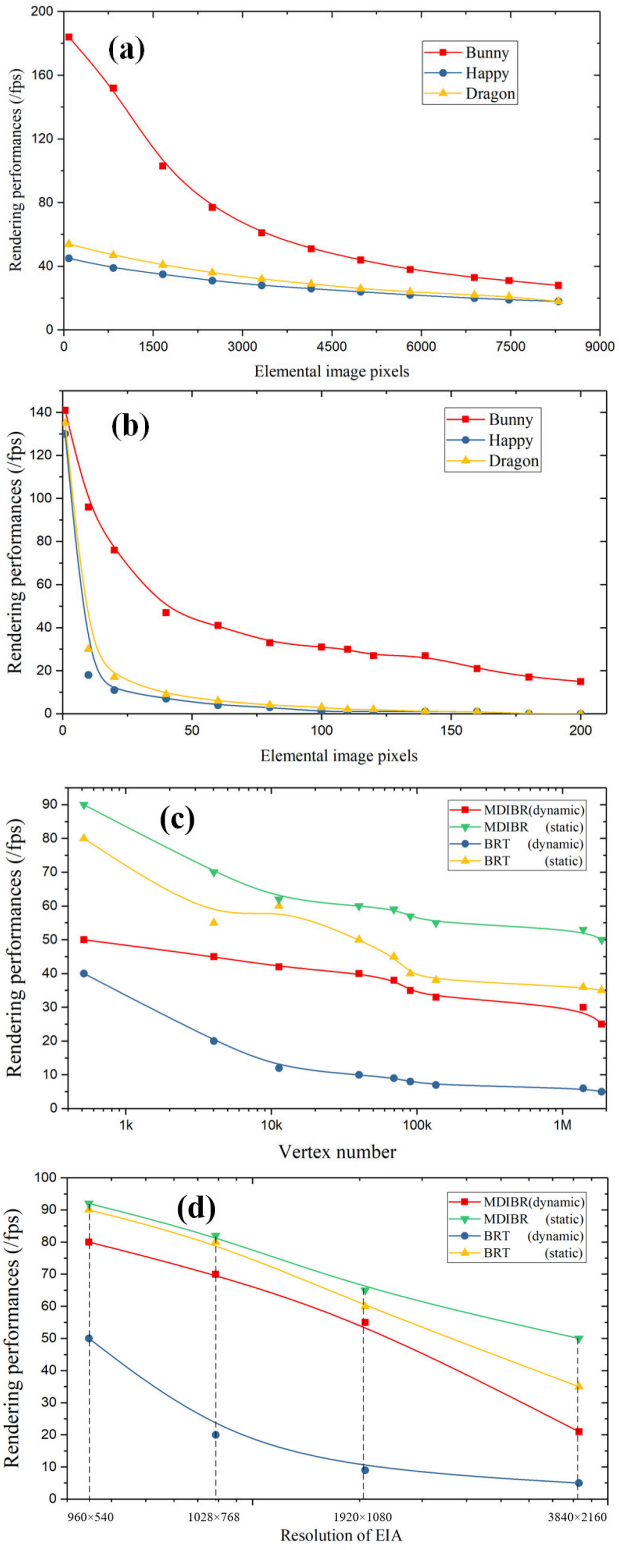

FIGURE 13. Generating performances (fps) of different rendering methods: (a) MDIBR method, (b) MVR method. The change of generating performances with (c) vertex number and (d) resolution of EIA.

cinematic pictures, as well as other kinds of digital images and videos [30]. SSIM is used for measuring the similarity between two images. The SSIM index is a full reference

FIGURE 14. The new viewpoint image calculated based on (a) 4 corners reference viewpoints, and (b) single reference viewpoint.

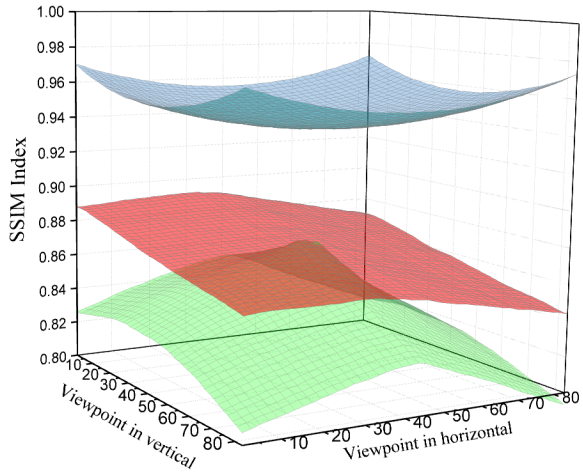

FIGURE 15. The SSIM values at different viewpoints.

metric; in other words, the measurement or prediction of the image quality is based on an initial uncompressed or distortion-free image as reference. The SSIM index is based on the computation of three terms, luminance term, contrast term and structural term, and ratio is 1:1:1. Calculation results of MDIBR and DIBR methods are compared as shown in Figure 14. The position of the destination viewpoint is at left 15° and down 15° to the center viewpoint. The image generated with the MDIBR method based on reference viewpoints with 4 corners is shown in Figure 14(a), the image generated with the MDIBR method without hole fulling is shown in Figure 14(b), and the image generated with the traditional DIBR method based on the single reference viewpoint is shown in Figure 14(c). Compared with the traditional DIBR method, the generated image with the MDIBR method has fewer holes and higher SSIM values. Some of the holes appearing in the destination viewpoint based on one reference viewpoint can be complemented by the corresponding non-hole region in the other reference viewpoint. The hole fulling further improves image quality.

The SSIM index is a method to predict the perceived quality of pictures. All SSIM values are compared for 80×80 viewpoint images, and the resolution of these images is 480×270. As shown in Figure 15, the blue grid represents the MDIBR, the red grid represents the MDIBR without hole fulling and the green grid represents the single viewpoint DIBR. We can see that the calculation results of MDIBR show

higher SSIM values, which means that the result based on MDIBR is more accurate.

IV. CONCLUSION

In summary, a real-time CGII display method based on MDIBR is presented. With the GPU acceleration, the computation time is greatly reduced, which makes it possible to realize real-time 3D elemental array generation with higher resolution. In the experiment, an interactive integral imaging display system based on the MDIBR method with an EIA resolution of 3840×2160 is demonstrated. The number of viewpoints in the optical experimental system reaches 80×80 and the frame rate rises above 25 fps. With the demonstrated method, the integrated imaging display system can realize an interactive real-time true 3D display.

REFERENCES

[1] M. Martínez-Corral and B. Javidi, "Fundamentals of 3D imaging and displays: A tutorial on integral imaging, light-field, and plenoptic systems," *Adv. Opt. Photon.*, vol. 10, no. 3, pp. 512–566, Sep. 2018, doi: 10.1364/AOP.10.000512.

[2] H. E. Ives, "Optical properties of a lippmann lenticulated sheet," *J. Opt. Soc. Amer.*, vol. 21, no. 3, pp. 171–176, Jan. 1931, doi: 10.1364/JOSA.21.000171.

[3] J.-H. Park, K. Hong, and B. Lee, "Recent progress in three-dimensional information processing based on integral imaging," *Appl. Opt.*, vol. 48, no. 34, pp. H77–H94, Dec. 2009, doi: 10.1364/AO.48.000H77.

[4] X. Sang, X. Gao, X. Yu, S. Xing, Y. Li, and Y. Wu, "Interactive floating full-parallax digital three-dimensional light-field display based on wavefront recomposing," *Opt. Express*, vol. 26, no. 7, pp. 8883–8889, Apr. 2018, doi: 10.1364/OE.26.008883.

[5] M. Cho, M. Daneshpanah, I. Moon, and B. Javidi, "Three-dimensional optical sensing and visualization using integral imaging," *Proc. IEEE*, vol. 99, no. 4, pp. 556–575, Apr. 2011, doi: 10.1109/JPROC.2010.2090114.

[6] Y. Igarashi, H. Murata, and M. Ueda, "3-D display system using a computer generated integral photograph," *Jpn. J. Appl. Phys.*, vol. 17, no. 9, pp. 1683–1684, Sep. 2014.

[7] H. Liao, T. Dohi, and K. Nomura, "Autostereoscopic 3D display with long visualization depth using referential viewing area-based integral photography," *IEEE Trans. Vis. Comput. Graphics*, vol. 17, no. 11, pp. 1690–1701, Nov. 2011, doi: 10.1109/TVCG.2010.267.

[8] K. Yanaka, "Integral photography using hexagonal fly's eye lens and fractional view," *Proc. SPIE*, vol. 6803, Feb. 2008, Art. no. 68031K, doi: 10.1117/12.766247.

[9] M. Halle, "Multiple viewpoint rendering," in *Proc. 25th Annu. Conf. Comput. Graph. Interact. Techn.*, Mar. 1996, pp. 243–254, doi: 10.1145/280814.280884.

[10] S.-W. Min, J. Kim, and B. Lee, "New characteristic equation of three-dimensional integral imaging system and its applications," *Jpn. J. Appl. Phys. Lett.*, vol. 44, no. 2, pp. L71–L74, Jan. 2005.

[11] R. Yang, X. Huang, and S. Chen, "Efficient rendering of integral images," in *Proc. 32nd Annu. Conf. Comput. Graph. Interact. Techn. (SIGGRAPH)*, Aug. 2005, p. 44, doi: 10.1145/1186954.1187005.

[12] S.-W. Min, K. S. Park, B. Lee, Y. Cho, and M. Hahn, "Enhanced image mapping algorithm for computer-generated integral imaging system," *Jpn. J. Appl. Phys.*, vol. 45, no. 28, pp. L744–L747, Feb. 2006.

[13] B.-N.-R. Lee, Y. Cho, K. S. Park, S.-W. Min, J.-S. Lim, M. C. Whang, and K. R. Park, "Design and implementation of a fast integral image rendering method," in *Proc. Int. Conf. Entertainment Comput.*, Sep. 2006, pp. 135–140, doi: 10.1007/11872320_16.

[14] K. S. Park, S.-W. Min, and Y. Cho, "Viewpoint vector rendering for efficient elemental image generation," *IEICE Trans. Inf. Syst.*, vol. E90-D, no. 1, pp. 233–241, Jan. 2007, doi: 10.1093/ietisy/e90-1.1.233.

[15] K.-C. Kwon, C. Park, M.-U. Erdenebat, J.-S. Jeong, J.-H. Choi, N. Kim, J.-H. Park, Y.-T. Lim, and K.-H. Yoo, "High speed image space parallel processing for computer-generated integral imaging system," *Opt. Express*, vol. 20, no. 2, pp. 732–740, 2012.

[16] D.-H. Kim, M.-U. Erdenebat, K.-C. Kwon, J.-S. Jeong, J.-W. Lee, K.-A. Kim, N. Kim, and K.-H. Yoo, "Real-time 3D display system based on computer-generated integral imaging technique using enhanced ISPP for hexagonal lens array," *Appl. Opt.*, vol. 52, no. 34, pp. 8411–8418, 2013.

[17] S. Jiao, X. Wang, M. Zhou, W. Li, T. Hong, D. Nam, J.-H. Lee, E. Wu, H. Wang, and J.-Y. Kim, "Multiple ray cluster rendering for interactive integral imaging system," *Opt. Express*, vol. 21, no. 8, pp. 10070–10086, Apr. 2013.

[18] S.-L. Li, Q.-H. Wang, Z.-L. Xiong, H. Deng, and C.-C. Ji, "Multiple orthographic frustum combing for real-time computer-generated integral imaging system," *J. Display Technol.*, vol. 10, no. 8, pp. 704–709, Aug. 2014, doi: 10.1109/JDT.2014.2315665.

[19] S. Xing, X. Sang, X. Yu, C. Duo, B. Pang, X. Gao, S. Yang, Y. Guan, B. Yan, J. Yuan, and K. Wang, "High-efficient computer-generated integral imaging based on the backward ray-tracing technique and optical reconstruction," *Opt. Express*, vol. 25, no. 1, pp. 330–338, Jan. 2017, doi: 10.1364/OE.25.000330.

[20] B. Pang, X. Sang, S. Xing, X. Yu, D. Chen, B. Yan, K. Wang, C. Yu, B. Liu, C. Cui, Y. Guan, W. Xiang, and L. Ge, "High-efficient rendering of the multi-view image for the three-dimensional display based on the backward ray-tracing technique," *Opt. Commun.*, vol. 405, pp. 306–311, Dec. 2017, doi: 10.1016/j.optcom.2017.08.013.

[21] H. Shum and S. B. Kang, "Review of image-based rendering techniques," *Proc. SPIE*, vol. 4067, pp. 2–13, May 2000.

[22] L. McMillan, "An image-based approach to three-dimensional computer graphics," Ph.D. dissertation, Dept. Comput. Sci., Univ. North Carolina, Chapel Hill, NC, USA, 1997.

[23] W. R. Mark, "Post-rendering 3D image warping: Visibility, reconstruction, and performance for depth-image warping," Ph.D. dissertation, Dept. Comput. Sci., Univ. North Carolina, Chapel Hill, Chapel Hill, NC, USA, 1999.

[24] C. Fehn, "A 3D-TV system based on video plus depth information," in *Proc. 27th Asilomar Conf. Signals, Syst. Comput.*, vol. 2, Pacific Grove, CA, USA, 2003, pp. 1529–1533, doi: 10.1109/ACSSC.2003.1292241.

[25] S. Zhu and Y. Yu, "Intermediate view synthesis based on disparity estimation and image interpolation," in *Proc. Int. Conf. Comput. Sci. Inf. Process. (CSIP)*, Xi'an, Shaanxi, 2012, pp. 1035–1038, doi: 10.1109/CSIP.2012.6309033.

[26] C. Zhu and S. Li, "A new perspective on hole generation and filling in DIBR based view synthesis," in *Proc. 9th Int. Conf. Intell. Inf. Hiding Multimedia Signal Process.*, Beijing, China, 2013, pp. 607–610, doi: 10.1109/IIH-MSP.2013.156.

[27] S. Li, C. Zhu, and M.-T. Sun, "Hole filling with multiple reference views in DIBR view synthesis," *IEEE Trans. Multimedia*, vol. 20, no. 8, pp. 1948–1959, Aug. 2018, doi: 10.1109/TMM.2018.2791810.

[28] C. Zhu and S. Li, "Depth image based view synthesis: New insights and perspectives on hole generation and filling," *IEEE Trans. Broadcast.*, vol. 62, no. 1, pp. 82–93, Mar. 2016, doi: 10.1109/TBC.2015.2475697.

[29] J. D. Foley, A. van Dam, S. K. Feiner, and J. F. Hughes, "More general transformations," in *Computer Graphics: Principles and Practice*, 2nd ed. Boston, MA, USA: Addison-Wesley, 1991, pp. 207–208.

[30] Z. Wang, E. P. Simoncelli, and A. C. Bovik, "Multiscale structural similarity for image quality assessment," in *Proc. 27th Asilomar Conf. Signals, Syst. Comput.*, Pacific Grove, CA, USA, 2003, pp. 1398–1402.

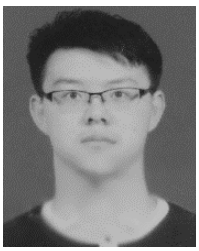

YANXIN GUAN received the B.S. degree in optical information science and technology from Qingdao University, in 2015. He is currently pursuing the Ph.D. degree with the Institute of Information Photonics and Optical Communications, Beijing University of Posts and Telecommunications, Beijing, China. His research interests include 3D display technologies and computer graphics.

XINZHU SANG received the dual bachelor's degrees in instrument science and management engineering from Tianjin University, Tianjin, China, in 1999, the M.S. degree from the Beijing Institute of Machinery, Beijing, China, in 2002, and the Ph.D. degree in physical electronics from the Beijing University of Posts and Telecommunications, Beijing, in 2005.

From December 2003 to March 2005, he was a Research Assistant with the Optoelectronics Research Centre, Department of Electronic Engineering, City University of Hong Kong. From July 2007 to July 2008, he was a Postdoctoral Research Scholar with the University of California at Irvine, Irvine, CA, USA. He is currently a Full Professor with the Beijing University of Posts and Telecommunications. His research interests include three-dimensional display, holography, and novel photonic devices. He is a Senior Member of the Chinese Institute of Communication and the Chinese Institute of Electronics. He is also the Secretary-General of the Committee of Holography and Optical Information, Chinese Optical Society Processing.

SHUJUN XING received the Ph.D. degree in electronic science and technology from the Institute of Information Photonics and Optical communications, Beijing University of Posts and Telecommunications, Beijing, China, in 2017. He is currently a Postdoctoral Researcher with the Department of Precision Instruments, Tsinghua University, Beijing. His major is in optical engineering and mainly study the 3D rendering method for special 3D display. His research interests include three-dimensional display, virtual reality, and multiview rendering.

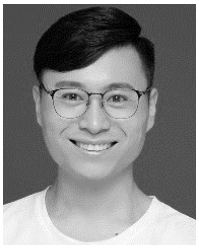

YUANHANG LI received the B.S. degree in communication engineering from Henan University, in 2016. He is currently pursuing the Ph.D. degree with the Institute of Information Photonics and Optical Communications, Beijing University of Posts and Telecommunications, Beijing, China. His research interests include 3D display technologies, computer graphics, medical image 3D display, and integral photography and its application in 3D display.

BINBIN YAN received the bachelor's degree in electronic science and technology and the Ph.D. degree in electromagnetic field and microwave technology from the Beijing University of Posts and Telecommunications, Beijing, China, in 2003 and 2010, respectively. From 2007 to 2009, she was supported by the scholarship of China Scholarship Council and sent to the Photonics and Optical Communications Group, University of New South Wales, Australia, as a Joint Doctoral Student. She is currently an Associate Professor with the State Key Laboratory of Information Photonics and Optical Communications, Beijing University of Posts and Telecommunications. She has published over 100 refereed articles. Her current interests are in the areas of 3D display devices, new optoelectronics devices, and optical information processing.